

A new imaging sign in COVID-19 pneumonia: vascular changes and their correlation with clinical severity of the disease

Deniz Esin Tekcan Şanlı 

Düzgün Yıldırım 

PURPOSE

It has come to our attention that specific vascular changes (VCs) appear more frequently in chest computed tomography (CT) of patients with coronavirus disease 2019 (COVID-19). In this study, we aimed to investigate if these specific VCs in chest CT correlate with clinical severity of the disease.

METHODS

CT images of 102 patients who underwent low-dose noncontrast chest CT due to COVID-19 between 11 March 2020 and 11 April 2020 were evaluated retrospectively. The patients were divided into two groups based on the presence of VCs in CT images. VCs in chest CT of patients with COVID-19 were defined using the following descriptors: decreased lumen caliber, vascular wall irregularity, angulation in the course of the vessel, vascular disruption, and/or interruption. The relationship of these VCs with disease symptoms (fever, cough, shortness of breath), comorbid conditions (diabetes, hypertension, asthma), smoking habit, disease-specific laboratory changes (white blood cell-lymphocyte count, neutrophil/lymphocyte ratio, C-reactive protein [CRP], D-dimer, lactate dehydrogenase [LDH], ferritin, procalcitonin), lung parenchymal infiltration pattern (ground-glass opacity, crazy-paving pattern, consolidation) and its distribution (peripheral, central, mixed, upper lobes, lower lobes, right middle lobe) on CT were investigated by comparison of these variables between patients with and without VCs in chest CT.

RESULTS

VCs were observed in 18 out of 102 patients (18%) with typical parenchymal involvement for COVID-19. There was no significant difference in terms of age and sex. We found an irregularity in the wall of the vascular structures in the distal branches and decreased lumen caliber of the vessels related to ground-glass opacities in 15 patients, concentric luminal narrowing in annular form in 4 patients, angulation/traction or springiness in the vascular structures towards the active lesions in 3 patients, and interruptions along the vascular course in 1 patient. VCs were significantly correlated with fever (12/18, 66.7%) and shortness of breath (7/18, 39%). These changes were significantly more remarkable in common disease involving both upper and lower lobes (10/18, 56%). In these cases, there was a substantial increase in CRP (15/18, 83%; mean, 5.7±6.3 mg/dL) and LDH (8/18, 44%) values compared to those who did not have any VCs.

CONCLUSION

The results of this study suggest that specific VCs observed in chest CT may predict the disease severity in cases of COVID-19 pneumonia. These changes may be related to respiratory distress in the disease.

From the Department of Radiology (D.E.T.Ş. ✉ tekcandenizesin@gmail.com), Acibadem Kozyatagi Hospital, Istanbul, Turkey; Department of Radiology (D.Y.), Acibadem Taksim Hospital, Istanbul, Turkey.

Received 13 May 2020; revision requested 10 June 2020; last revision received 18 June 2020; accepted 2 July 2020.

Published online 9 October 2020.

DOI 10.5152/dir.2020.20346

Coronavirus disease 2019 (COVID-19), caused by severe acute respiratory syndrome coronavirus 2 (SARS-CoV-2), is a severe infection primarily affecting the respiratory tract. The disease was first described in Wuhan, China, in December 2019, and then quickly spread most of the world, causing a disastrous pandemic (1, 2). COVID-19 pandemic has become an important public health problem in a relatively short time with its high mortality rate and collapsed social and economic life, globally. Although there is no proof of an effective treatment until now, there are a significant amount of studies focused on the mechanisms of transmission, clinical features, the most common laboratory and radiological findings, and the course of the disease (3).

You may cite this article as: Tekcan Şanlı DE, Yıldırım D. A new imaging sign in COVID-19 pneumonia: vascular changes and their correlation with clinical severity of the disease. *Diagn Interv Radiol* 2021; 27: 172–180

Radiological imaging methods, especially CT examination, have been widely used in the diagnosis of the disease since real-time RT-PCR is not widely available and the results may take a couple of days. Although it is not a screening tool, chest CT could provide valuable diagnostic information as stated by international radiological associations (4–7). Accordingly, it has also been shown that chest CT may predict the prognosis of the disease and guide clinicians for the best treatment strategy (6, 8).

Chest CT findings of the disease have been clearly classified as typical and atypical (3, 6). Bilateral or multilobar peripheral-subpleural and basal distribution of ground-glass opacities (GGOs) is the most common and typical finding for the disease (9–14). Apart from this, during the defined temporal evolution process of the disease, cobblestone pattern accompanied by interlobular septal thickening, consolidation areas, and fibrotic bands are also frequent findings with similar distribution (3, 15). There are some other chest CT findings specific to the disease such as vascular enlargement which is suggested to be due to the vasodilator effect of inflammatory cytokines at the level of active lesions, the air bubble sign (vacuolar sign) in the lesion during the healing process, GGOs surrounding central consolidated area (halo sign), and the reverse finding with consolidation surrounding the central GGO (reverse halo-atoll sign) (16, 17). Bronchial changes, such as bronchiectasis or deformation, have also been reported (3).

Pleural thickening-pleural effusion, cavitation-pneumothorax, mediastinal lymph nodes are considered as atypical findings that we rarely see and usually manifest as late-stage or complication findings (e.g., due to secondary infection, heart failure)

during the disease course. It is anticipated that the prognosis would be worse in patients who developed these findings at the beginning of the admission or during the course of the disease (3).

Our aim in this study is, in addition to presenting typical findings described for COVID-19 infection, to identify disease-specific VCs that have been not mentioned in the literature until now, and demonstrate radiological imaging features helpful for differential diagnosis. In addition, we aimed to evaluate the relationship between the VCs and disease symptoms, comorbidities, and laboratory findings, and examine the clinical-radiological correlation.

Methods

Study population

Local institutional review board approval was obtained for this study (2020-05/28), and informed consent forms was obtained prior to CT acquisition. A total of 102 patients who underwent chest CT between 11 March and 11 April and received subsequent treatment for COVID-19 in our hospital were included in this study. Diagnosis of COVID-19 was based on relevant clinical findings, chest CT images, and were confirmed with real-time RT-PCR test. Patients were classified into two groups based on their findings of VCs in chest CT.

Clinical and laboratory findings

Chart review for following information was performed and data were recorded: presence of high fever (over 37.5°C), cough, shortness of breath ($\text{PaO}_2 < 93$ or respiratory rate > 20), comorbidities (diabetes, hypertension, asthma) and smoking history. Disease-specific laboratory values including lymphocyte count, neutrophil/lymphocyte ratio (NLR), C-reactive protein (CRP), D-dimer, lactate dehydrogenase (LDH), ferritin, procalcitonin were also included.

CT examination

All CT scans were performed with Siemens Somatom Sensation-SyngoCT 2009 device using a low-dose CT protocol. Patients were scanned in supine position during deep inspiration. The acquisition parameters were standardized as: tube voltage, 140 kV; tube current, 40 mA; pitch, 1.4; field of view (FOV), 455 mm; slice thickness, 64×0.6 mm. Obtained images were converted into 1 mm thin reconstructions in lung parenchymal window to evaluate the vascular signs, by

multi-plane remodeling in axial, coronal, and sagittal planes with B70 kernel limited to lung FOV. Maximum intensity projection (MIP) 8 mm images were also created in coronal, sagittal, and axial plans by post-processing procedures and sent to the PACS. Rules of isolation and disinfection during and after the scanning were strictly adhered. Mask and other personal protective equipment were mandatory for technicians, patients, and cleaning staff.

Image analysis

All images were evaluated separately by two radiologists with 20 years (D.Y.) and 10 years (N.E.) of experience in chest CT in the first evaluation. The findings were evaluated together in the secondary evaluation and discrepancies were resolved by consensus. Findings that are typical and atypical for the disease were classified according to the criteria of “A rapid advice guideline for the diagnosis and treatment of 2019 novel coronavirus infected pneumonia (standard version)” (3). Basal-peripheral distribution of GGOs, GGO and consolidation combination, interlobular septal thickening, crazy-paving pattern, subpleural lines, halo sign, reverse halo sign, vacuolar sign, vascular enlargement, and bronchial deformation were evaluated as typical findings; while, tree-in-bud view, lobar consolidation-bronchopneumonia, mediastinal lymphadenopathy, and pleural effusion-thickening were evaluated as atypical findings.

Radiologically typical-atypical presentations were evaluated according to the criteria of the Radiological Society of North America (RSNA) Expert Consensus Statement on Reporting Chest CT Findings Related to COVID-19, as of April 2020 (18).

Infiltration patterns were mainly in the form of GGO, crazy-paving pattern, consolidation. Their distributions were classified as peripheral (distal 1/3 of lung parenchyma), central, and diffuse. Location of lobar involvement, largest lesion diameter, and percentage of affected total lung parenchyma (scored as 1, $< 25\%$; 2, $25\%–50\%$; 3, $50\%–75\%$; 4, $> 75\%$) were reviewed.

Vascular changes criteria

The inclusion criteria for the vascular changes was infiltration in the form of GGO or in a crazy-paving pattern in COVID-19 patients.

The criteria for exclusion were cases over 65 years of age (since age-related vascular changes will be expected in el-

Main points

- CT has a high sensitivity and specificity in the diagnosis of COVID-19 pneumonia.
- Chest CT imaging features have predictive value for the prognosis of the disease.
- Chest CT imaging features can manifest with typical and atypical findings.
- Vascular changes may also be observed during the early course of the disease, as well as bronchial and parenchymal involvement.
- Vascular changes may be an indicator of respiratory distress caused by the illness.

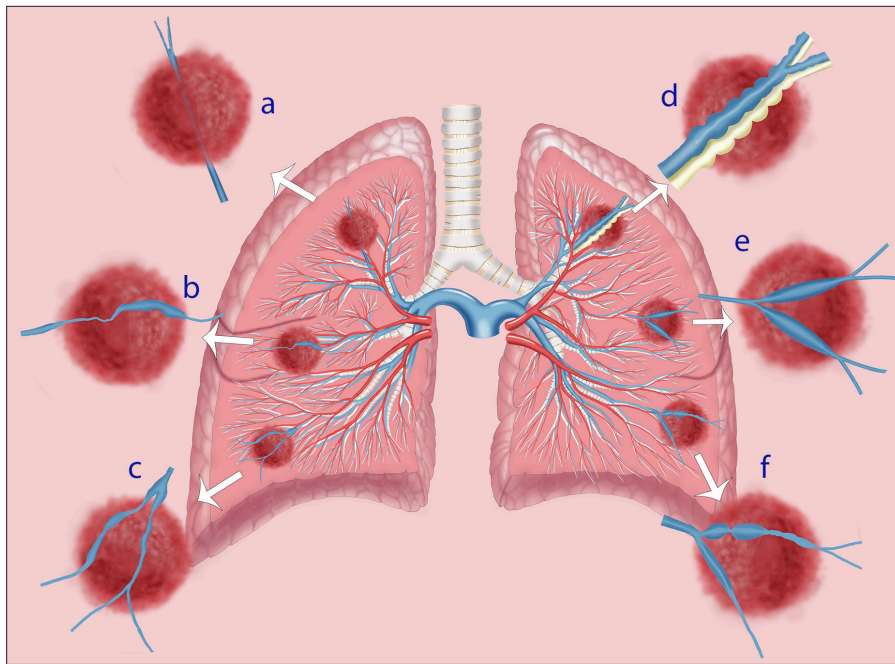


Figure 1. Schematic representation of vascular changes: a, invisible vessel-vascular thinning; b, vascular angulation-traction; c, vascular wall irregularity; d, bronchovascular ectasia; e, vascular enlargement; f, vascular knuckle-annular contraction.

	Vascular changes, n (%)		p
	Positive	Negative	
Fever	12 (66.7)	35 (41.7)	0.053 ^a
Shortness of breath	7 (38.9)	12 (14.3)	0.039 ^b
Cough	16 (88.9)	56 (66.7)	0.060 ^a

^aPearson chi-square test; ^bFisher's exact test.

derly patients), patients who have received radiotherapy before (because it causes pulmonary structural changes and fibrosis affecting vessels), infiltration pattern in the form of consolidation (since vascular structures cannot be visualized in consolidation areas with non-contrast CT), bronchiectasia (chronic bronchiectasis changes will be accompanied by vascular changes), and coexisting background parenchymal lung disease such as chronic obstructive pulmonary disease (COPD), emphysema (likewise, as the vascular bed is affected in chronic parenchymal lung diseases).

Vascular thinning or "vasospasm" was used to define 20% reduction of the vessel diameter at the level of infiltration area compared to the distal segment of the vessel, or if vascular branches cannot be observed in a bronchial bundle in its distal course. A 30-degree shift of vessel course

from its normal straight course was considered as angulation. Vascular knuckle was used to define an annular segmental concentric narrowing of the vessel; vascular irregularity, for irregular course at the level of infiltration or if there is an irregularity in the vessel wall; bronchovascular changes, for changes such as ectasia-deformation (Fig. 1). All these changes were evaluated on multiplanar images to prevent overdiagnosis.

Statistical analysis

NCSS (Number Cruncher Statistical System) 2007 software was used for statistical analysis. Mann Whitney U test was used for continuous variables. Pearson chi-square test, Fisher's exact test, and Fisher Freeman Halton tests were used for categorical data. $p < 0.05$ was considered significant. Interobserver reliability of evaluation of the vascular changes was analyzed.

Results

Of the 102 patients included in the study, 72% (n=73) were male, and 28% (n=29) were female. The age range was 19–94 years, with a mean and standard deviation of 48.62 ± 14.42 years.

Evaluation of vascular enlargement and bronchial deformation findings on CT revealed VCs such as tortuosity, deformation, irregularity, and angulation in 18 cases (18%) with a typical and diffuse infiltration pattern, in or near the affected area. Interobserver agreement was high as expressed by a kappa value of 0.9.

The age and sex distributions of these cases did not differ with regard to the presence of VCs ($p > 0.05$). Clinical presentations and laboratory data of the cases with and without VCs identified on chest CT differed significantly. Incidence of shortness of breath ($\text{PaO}_2 < 93\%$ or respiratory rate > 20) was significantly higher in patients with VCs compared to patients without VCs ($p = 0.039$). Presence of fever was remarkably more frequent in cases with VCs than those without, although the difference was not statistically significant ($p = 0.053$). No correlation was found between cough and VCs ($p > 0.05$) (Table 1).

Based on the presence of VCs, the incidence of diabetes, hypertension, and asthma did not differ statistically ($p > 0.05$). However, smoking rate was significantly higher in cases with VCs ($p = 0.044$). The risk of VCs in smoking patients was higher with an odds ratio of 3.5 (95% CI, 1.138–10.764) (Table 2). The association of vascular changes with emphysema or COPD was not evaluated in these patients, since chronic lung diseases that may be related to vascular damage constituted an exclusion criterion in this study.

Presence of VCs did not show statistically significant correlation with lymphocyte count, NLR, ferritin, D-dimer, and procalcitonin levels. However, CRP ($p = 0.008$) and LDH ($p = 0.011$) values were significantly higher in cases with VCs than those without (Table 3). The average CRP value in cases with VCs was quite high, with a mean level of 5.7 ± 6.3 mg/L.

All of the cases with VCs showed the typical pneumonic infiltration pattern of COVID-19. A positive correlation was found between the diameter of the lesions (larger than 5 cm) and VCs ($p = 0.01$). The presence of diffuse lesions centrally in addition to peripheral location correlated with VCs ($p = 0.04$). The risk of VC in right middle lobe

	Vascular changes, n (%)		<i>p</i> ^a
	Positive	Negative	
Diabetes	3 (16.7)	9 (10.7)	0.440
Hypertension	4 (22.2)	16 (19.0)	0.749
Asthma	1 (5.6)	3 (3.6)	0.546
Smoking	7 (41.2)	14 (16.7)	0.044
Other diseases	1 (5.6)	3 (3.6)	0.546

^aFisher's exact test.

		Vascular changes, n (%)		<i>p</i>
		Positive	Negative	
Low lymphocyte count (<1300)		9 (50.0)	22 (41.5)	0.530 ^a
NLR	>3	8 (47.1)	18 (34.0)	0.331 ^a
CRP	Normal	1 (5.9)	20 (40.8)	0.008
	High	16 (94.1)	29 (59.2)	
D-dimer	Normal	3 (30.0)	2 (12.5)	0.340 ^b
	High	7 (70.0)	14 (87.5)	
LDH	Normal	9 (50.0)	69 (82.1)	0.011 ^b
	High	9 (50.0)	15 (17.9)	
Ferritin	Normal	0 (0.0)	5 (26.3)	0.128 ^b
	High	12 (100.0)	14 (73.7)	
Procalcitonin	Normal	4 (40.0)	5 (26.3)	0.675 ^b
	High	6 (60.0)	14 (73.7)	

NLR, neutrophil lymphocyte ratio; CRP, C-reactive protein; LDH, lactate dehydrogenase.
^aPearson chi-square test; ^bFisher's exact test.

		Vascular changes, n (%)		<i>p</i>
		Positive	Negative	
GGO		18 (100.0)	79 (94.0)	0.583 ^a
Crazy-paving pattern		11 (61.1)	21 (25.0)	0.003 ^b
Consolidation		6 (33.3)	23 (27.4)	0.611 ^b
Right upper lobe		14 (77.8)	43 (54.4)	0.110 ^a
Left upper lobe		14 (77.8)	39 (49.4)	0.029 ^b
Right middle lobe		10 (55.6)	21 (26.6)	0.017 ^b
Right lower lobe		17 (94.4)	63 (79.7)	0.183 ^a
Left lower lobe		16 (88.9)	62 (78.5)	0.512 ^a
Distribution	Peripheral	3 (16.7)	39 (49.4)	0.004 ^b
	Central	0 (0.0)	8 (10.1)	0.004 ^b
	Mixed	15 (83.3)	32 (40.5)	

GGO, ground-glass opacity.
^aFisher's exact test; ^bPearson chi-square test.

infiltrations was higher than in infiltrations elsewhere ($P = 0.017$). Presence of VCs was correlated with larger number of affected

lobes (> 2 lobes affected, $P = 0.005$) and larger area of lung parenchyma affected (>50%, $P = 0.029$) (Table 4).



Figure 2. In the typical infiltration pattern for COVID-19, vascular structures can be identified distally among GGOs with peripheral subpleural-basal distribution in bilateral lower lobes.

Of the patients with VCs, 55% (10/18) were hospitalized; the average hospitalization duration was 7 days (range, 1–15 days) and one patient required intensive care for 15 days. In the patient group without VCs, hospitalization rate was 28%; the average hospitalization duration was 5 days (3–13 days) and 4 patients required intensive care (4/84, 5%) for an average of 10 days (2–35 days). The hospitalization rate, length of hospital stay, and need for intensive care was significantly higher in the group with VCs than those without.

None of the patients with VCs had a chest CT image taken in our clinic before COVID-19 pneumonia. There was no follow-up CT taken after the disease except for two patients. In these patients, parenchymal findings related to COVID-19 mostly regressed at follow-up CT. Vascular changes such as irregularity and thinning that we saw in the ground-glass opacities also completely regressed in the follow-up CT.

Apart from these, typical CT findings for COVID-19 included halo sign 14% (n=14), reverse halo sign 9% (n=9), vascular enlargement 10% (n=10), bronchial changes 3% (n=3), and vacuolar sign 2% (n=2).

In interobserver reliability analysis, VC evaluation was highly reproducible (kappa value, 0.89). All VCs described in the study are schematized in Fig. 1. Normal vascular structures in the infiltration areas with GGO are seen in Fig. 2.

Fig. 3 shows dimmed and thinned vascular structures possibly due to the vasoconstrictor effects of cytokines. Fig. 4 shows that vascular structures narrowed concentrically in annular formation. This may be secondary to vasoconstriction, and focal

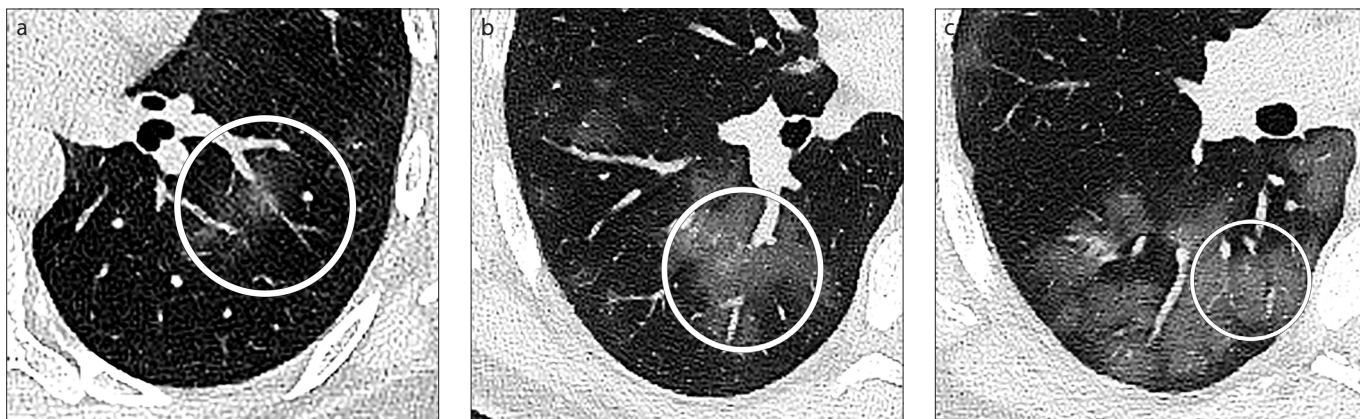


Figure 3. a–c. Images (a–c) show invisible vessels. Notice the faded-thinned or non-visualized vascular structures in the center of the active GGO lesions. These appear normal in the normal lung parenchyma after the lesion.

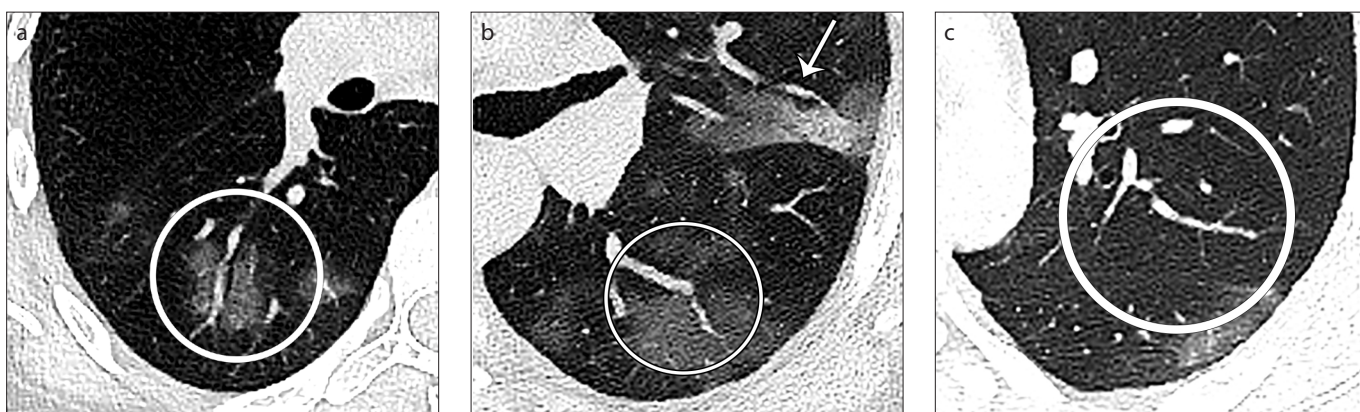


Figure 4. a–c. Images (a, b) show concentric narrowing in vascular structures within an active GGO. Image (c) shows concentric luminal narrowing and subsequent wall irregularity in the vascular structures remaining more proximally in a patient with residual infiltrative lesions in the posterobasal area.

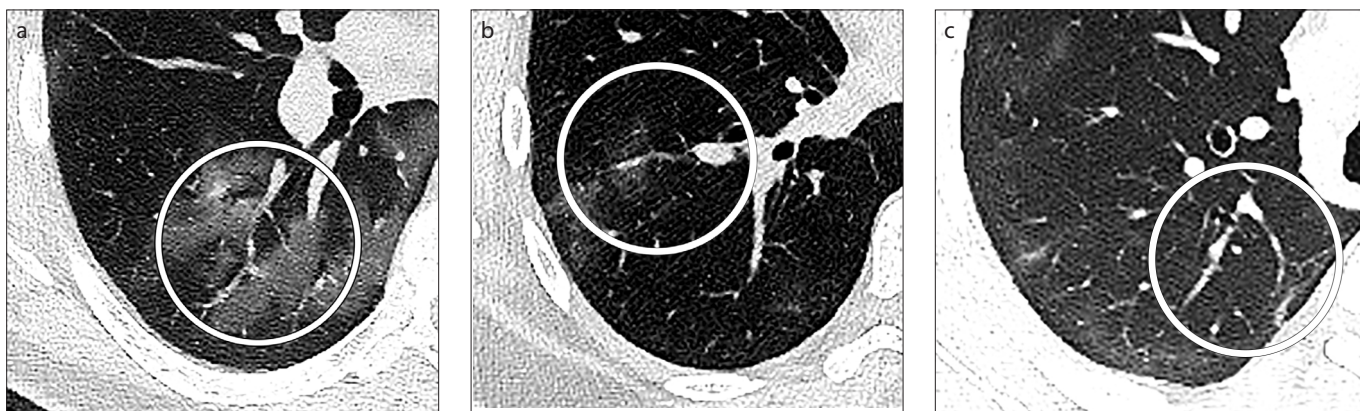


Figure 5. a–c. Images (a–c) show thinning, fading, irregularity of the vascular structures in or adjacent to an active lesion.

thrombosis caused by local inflammatory cytokines. Fig. 5 shows thinning, fading, and irregularity of the vascular structures in or adjacent to the active lesion.

In Fig. 6, the vascular structures are seen spreading towards the active GGO lesion; there is slight vascular angulation and irregularity in the crazy-paving pattern, which

we see as a mid-stage finding, and a sharp vascular angulation by the fibrotic process within the more dense lesion at the stage of possible chronic inflammation. Fig. 7 shows the pulmonary vascular structures that we define as a vascular interruption, whose continuity cannot be selected as segmental. Fig. 8a shows a case that was excluded from the

study because of tubular bronchiectatic lung disease; we see the VCs similarly in the form of constrictions-dilatations which we consider as resorption stage of the disease with residual lung parenchymal findings such as fibrous bands and faint GGOs. In Fig. 8b, although it is not very clear, we see vascular narrowing-dilatations accompanied by COVID-19-related

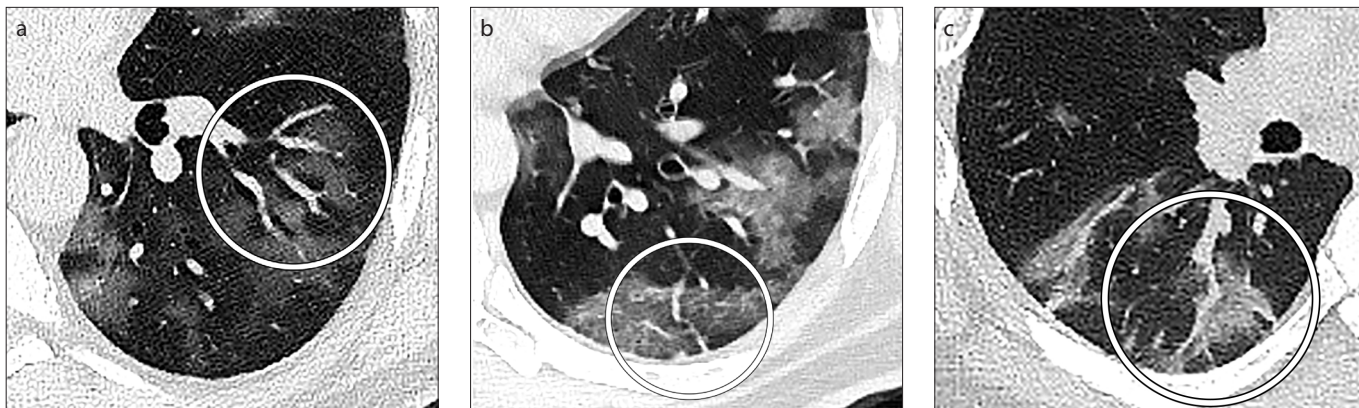


Figure 6. a–c. Images (a–c) show springiness-angulation-traction in the vascular structures in infiltrative lesions in the form of GGOs, crazy-paving, and consolidation at different stages of the disease.

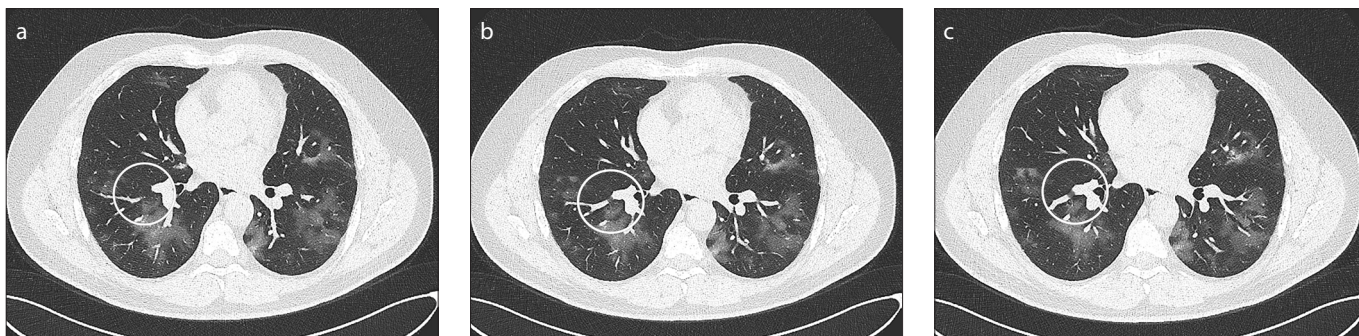


Figure 7. a–c. Serial images (a–c) of vascular interruption: segmental disruption in vascular continuity (circle), invisible vessel (arrow).

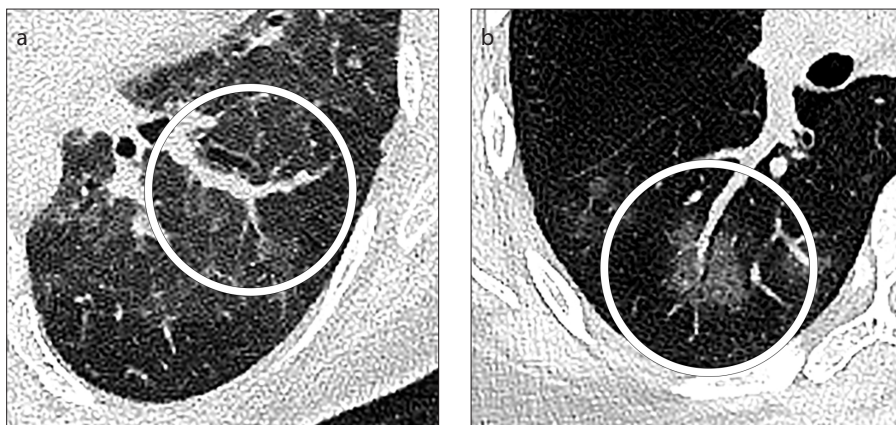


Figure 8. a, b. Bronchovascular changes: (a), changes in vascular structures in a patient with chronic bronchiectasis; (b), mild bronchovascular ectatic changes in a patient with disease-related active GGO lesion.

mild bronchial changes in the lesion with active GGO in the right lower lobe.

Vascular structures cannot be clearly selected within the crazy-paving pattern (Fig. 9a, 9b); similarly, vascular structures within the consolidations cannot be evaluated without contrast (Fig. 9c).

Discussion

SARS-CoV-2 affected the world in a short period of 5 months, causing a pandemic.

It is well known that the virus primarily affects the respiratory tract and, radiological findings have a high diagnostic value as well as a prognostic value (3, 19). The lung damage caused by the virus is reflected in the radiological imaging findings which has been described in detail in the literature studies and guidelines so far (3, 6–10, 20, 21). Advanced age, male sex, and comorbid diseases are poor prognostic factors for COVID-19 (3, 21). In addition, patients who

show extensive infiltration of atypical imaging findings in the form of consolidation at the time of first hospital admission are more likely to show progression and require hospitalization or intensive care.

As known, inflammation is a defense mechanism initiated against microbial or cytotoxic agents. With the influence of pro-inflammatory cytokines such as interleukin-1, tumor necrosis factor- α , nitric oxide, and prostaglandins dominating the early inflammatory process, vascular permeability increases secondary to vasodilation, and edema-exudate occurs in the intercellular space (22). With mediators activated by endothelial damage caused by the inflammatory reaction, reflex vasoconstriction occurs, and the coagulation cascade begins. As stated by Marini et al. (23), the ventilation-perfusion balance is disturbed by endothelial damage effect of inflammation and edema formed at the alveolar level and interalveolar space; this affects blood-oxygenation, creates hypoxia and activates mediators such as protein kinase C, which triggers pulmonary arterial vasoconstriction with a lung-specific mechanism (23). If this condition becomes severe or permanent, acute respiratory distress



Figure 9. a–c. In images (a, b), vascular changes cannot be clearly visualized in intermediate stage cases with crazy-paving pattern. As shown in image (c), vascular structures cannot be clearly distinguished in the consolidation areas, but accompanying vascular changes may be predicted when there are bronchial structural changes that can be distinguished as air bronchograms in a consolidation.

syndrome (ARDS), pulmonary hypertension, and heart failure may develop clinically (23–25).

The inflammatory reaction initiated by the virus, damaging the distal airways, especially at the alveolar level by these cytokines differs from person to person, varying by age, sex, duration of the inflammatory process, and the balance of pro-inflammatory/anti-inflammatory response (26, 27). Edema-exudate secondary to the inflammatory cascade appears as GGO, where the background parenchymal structures and vascular formations can be visualized radiologically (28) (Fig. 2). Vascular dilatation, which also occurs through the same mediators, may be visualized as vascular enlargement, and a typical finding for the disease on CT is the starting point of all these VCs. Although the most known and prominent vascular change specific to the disease is vascular enlargement, it should be kept in mind that vasoconstriction may be seen concurrently due to anti-inflammatory cytokines and thrombotic mediators, resulting in irregularity of vessel wall, decreased caliber or interruption of the vessel course (23, 29).

A large part of the VCs that we described could be explained with the physiological processes mentioned above, in the acute inflammation phase during the early disease period in the form of active GGO within the infiltration areas or adjacent tissue. Based on the results we obtained in this study, we think that as the prevalence of GGO and the area of the affected lung parenchyma increases, the possibility of these VCs will increase. In some of these active lesions, vascular structures may become

dimmed, possibly due to the vasoconstrictor effects of cytokines (Fig. 3). Even seldom, this vasospasm can be so evident that vascular structures within the lesion are never visualized and reappear at the normal parenchyma level.

As supported by the physiological inflammatory processes, we consider that the traction/angulation finding in vascular structures mediated by the fibrotic mediators dominating the infiltration region within the subacute-chronic inflammatory process seen in second or third weeks, are corresponding to the subacute and late stages of disease process. In other words, we think that visual findings on CT in the temporal evolution of COVID-19 and the physiological stages of inflammation are correlated. Findings such as traction bronchiectasis, bronchial deformation-contraction, which occur when fibrotic changes affect the bronchi in severe and prolonged inflammation, are reported as typical for the disease. In this context, considering their histological structures, we estimate that pulmonary arterial and especially pulmonary venous structures with thinner muscular layers will be more sensitive to these locally and systemically effective mediator-mediated changes than bronchi, and VCs may be seen more frequently than bronchial changes (30).

These findings described above, were not uncommon, especially when examined carefully in thin-section multiplanar imaging, and were identified in 18/102 (18%) cases. This was at a much higher rate than the findings considered typical for the disease such as bronchial deformation, vacuolar sign, and reverse halo sign. Therefore,

while evaluating CT examinations, VCs, which we can consider as typical for the disease, should be searched among the other findings (Figs. 3–8).

We could not find VCs in the infiltration areas with a crazy-paving pattern or consolidation, which we often encounter as an intermediate-late stage disease image on CT (Fig. 9). The reason for this may be that there are no obvious visible VCs in the late period of the disease, which corresponds to a pro-anti-inflammatory balance. Also, as these patterns are denser than GGO, they may hide the existing VCs. Although this situation is a limitation for the vascular sign, existing bronchial changes will help us at this stage (31). According to our results, if a bronchial deformation is seen, we can say that VCs have also developed (32–35).

In our study, we also evaluated the correlation of these identified changes with disease-specific clinical, laboratory, and radiological findings. We have shown that these changes are statistically significantly more frequent in smokers. The reason for this may be that endothelial damage caused by smoking is triggered by active inflammatory processes and causes vascular damage. We also statistically showed that CRP value, which demonstrates the severity of inflammation, is related to VCs. Again, we found a positive correlation between fever, which is a response of the body to this inflammatory reaction, and VCs. We found that the VCs are more extensive involving not only the peripheral lung parenchyma but also centrally, affecting the upper lobes and infiltrating more than 50% of the lung parenchyma. The statistical findings support the argument that the defined VCs are

formed under the influence of inflammatory mediators. As the extent of the disease increases, the immune reaction and released mediators will also increase and will predispose to the development of VCs.

Although it has been the subject of many studies, permanent or advanced parenchymal findings of COVID-19 disease have not been clarified yet. Perhaps, within the new indications that may occur over time, permanent damage and changes in vascular structures can be evaluated more clearly if chest CT scans are taken with contrast. Our results suggest that the disruption of the pulmonary vascular bed, ventilation-perfusion mismatch, and blood-oxygenation imbalance caused by these VCs could be related to the respiratory distress that is faced mostly in the acute period of the disease in severe cases. Shortness of breath, which is a common clinical finding in COVID-19 pneumonia, was correlated with the VCs in our study. In this context, there is a need for clinical studies that reveal the relationship of the respiratory stress, ARDS, and heart failure with VCs. Clinical and radiological studies that reveal the importance of VCs in predicting the prognosis and progression of the disease may pave the way for more effective management strategies, and perhaps the use of vascular drugs may be considered in the symptomatic treatment of the disease.

The major limitation of this study is the lack of intravenous contrast, which limits the assessment of vascular structures. On the other hand, we did not have image quality issues on evaluating these vascular structures with the help of iterative reconstructions and thin-section multiplanar reconstructions that we routinely use in our center to improve low-dose CT image quality. Contrast injection would make it easier to determine and evaluate VCs. However, using the contrast adds a potential risk to an already complicated disease course.

In conclusion, our findings reveal a relation between the extent of the disease, immune reaction, and the presence of vascular signs indicating that there is involvement of the vascular system in COVID-19 pneumonia. In addition to the typical findings, disease-related VCs should be considered in the evaluation of chest CT examinations taken for COVID-19.

Acknowledgment

We thank Dr. Ahmet Necati Şanlı for the medical illustration.

Conflict of interest disclosure

The authors declared no conflicts of interest.

References

1. Wang C, Horby PW, Hayden FG, Gao GF. A novel coronavirus outbreak of global health concern. *Lancet* 2020; 395:470–473. [\[Crossref\]](#)
2. Singhal T. A review of coronavirus disease-2019 (COVID-19). *Indian J Pediatr* 2020; 87:281–286. [\[Crossref\]](#)
3. Jin YH, Cai L, Cheng ZS, et al. A rapid advice guideline for the diagnosis and treatment of 2019 novel coronavirus (2019-nCoV) infected pneumonia (standard version). *Mil Med Res* 2020; 7:1–24. [\[Crossref\]](#)
4. Salehi S, Abedi A, Balakrishnan S, Gholamrezanezhad A. Coronavirus disease 2019 (COVID-19): a systematic review of imaging findings in 919 patients. *Am J Roentgenol* 2020 Feb 29. [Epub Ahead of Print] [\[Crossref\]](#)
5. Kim JY, Choe PG, Oh Y, et al. The first case of 2019 novel coronavirus pneumonia imported into Korea from Wuhan, China: implication for infection prevention and control measures. *J Korean Med Sci* 2020 Feb 3. [Epub Ahead of Print] [\[Crossref\]](#)
6. Pan Y, Guan H, Zhou S, et al. Initial CT findings and temporal changes in patients with the novel coronavirus pneumonia (2019-nCoV): a study of 63 patients in Wuhan, China. *Eur Radiol* 2020 Feb 13. [Epub Ahead of Print] [\[Crossref\]](#)
7. Amalou A, Türkbey B, Sandford T, et al. Targeted early chest CT in COVID-19 outbreaks as diagnostic tool for containment of the pandemic - A multinational opinion. *Diagn Interv Radiol* 2020 Apr 22. [Epub Ahead of Print]
8. Ding X, Xu J, Zhou J, Long Q. Chest CT findings of COVID-19 pneumonia by duration of symptoms. *Eur J Radiol* 2020 Apr 18. [Epub Ahead of Print] [\[Crossref\]](#)
9. Fang Y, Zhang H, Xu Y, Xie J, Pang P, Ji W. CT manifestations of two cases of 2019 novel coronavirus (2019-nCoV) pneumonia. *Radiology* 2020; 295:208–209. [\[Crossref\]](#)
10. Lei J, Li J, Li X, Qi X. CT imaging of the 2019 novel coronavirus (2019-nCoV) pneumonia. *Radiology* 2020; 295:18. [\[Crossref\]](#)
11. Shi H, Han X, Zheng C. Evolution of CT manifestations in a patient recovered from 2019 novel coronavirus (2019-nCoV) pneumonia in Wuhan, China. *Radiology* 2020; 295:20. [\[Crossref\]](#)
12. Chan JFW, Yuan S, Kok KH, et al. A familial cluster of pneumonia associated with the 2019 novel coronavirus indicating person-to-person transmission: a study of a family cluster. *Lancet* 2020; 395:514–523. [\[Crossref\]](#)
13. Zhang Z, Li X, Zhang W, Shi Z-L, Zheng Z, Wang T. Clinical features and treatment of 2019-nCoV pneumonia patients in Wuhan: report of a couple cases. *Virology* 2020 Feb 07. [Epub Ahead of Print] [\[Crossref\]](#)
14. Xu X, Yu C, Zhang L, Luo L, Liu J. Imaging features of 2019 novel coronavirus pneumonia. *Eur J Nucl Med Mol Imaging* 2020; 47:1022–1023. [\[Crossref\]](#)
15. Li L, Ren MJ, Zhang YY, Li WQ, Zhao HY, Liang LC. Lung CT image of a confirmed case of the 2019 novel coronavirus (2019-nCoV) infected pneumonia (with differential diagnosis of the SARS). *Yixue Xinzhi* 2020; 30:4–6.
16. Zhou S, Wang Y, Zhu T, Xia L. CT features of coronavirus disease 2019 (COVID-19) pneumonia in 62 patients in Wuhan, China. *Am J Roentgenol* 2020 Mar 5. [Epub Ahead of Print] [\[Crossref\]](#)
17. Bekçi T. "Reversed halo sign" on 3D CT in COVID-19. *Diagn Interv Radiol* 2020 Apr 30. [Epub Ahead of Print] [\[Crossref\]](#)
18. Simpson S, Kay FU, Abbara S, et al. Radiological Society of North America Expert Consensus Statement on Reporting Chest CT Findings Related to COVID-19. Endorsed by the Society of Thoracic Radiology, the American College of Radiology, and RSNA. *J Thorac Imaging*. 2020 Apr 28. [Epub Ahead of Print] [\[Crossref\]](#)
19. Fang Y, Zhang H, Xie J, et al. Sensitivity of chest CT for COVID-19: comparison to RT-PCR. *Radiology* 2020 Feb 19. [Epub Ahead of Print] [\[Crossref\]](#)
20. Wang Y, Dong C, Hu Y, et al. Temporal changes of CT findings in 90 patients with COVID-19 pneumonia: a longitudinal study. *Radiology* 2020 Mar 19. [Epub Ahead of Print] [\[Crossref\]](#)
21. Singh AK, Gupta R, Ghosh A, Misra A. Diabetes in COVID-19: Prevalence, pathophysiology, prognosis and practical considerations. *Diabetes Metab Syndr* 2020; 14:303–310. [\[Crossref\]](#)
22. Rankin, James A. Biological mediators of acute inflammation. *AACN Advanced Critical Care* 2004; 15:3–17. [\[Crossref\]](#)
23. Marini JJ, Gattinoni L. Management of COVID-19 Respiratory Distress. *JAMA* 2020 Apr 24. [Epub Ahead of Print] [\[Crossref\]](#)
24. Tsai BM, Wang M, Pitcher JM, Meldrum KK, Meldrum DR. Hypoxic pulmonary vasoconstriction and pulmonary artery tissue cytokine expression are mediated by protein kinase C. *Am J Physiol Lung Cell Mol Physiol* 2004; 287:L1215–1219. [\[Crossref\]](#)
25. Pahwa R, Jialal I. Chronic inflammation. [Updated 2019 Jun 4]. *StatPearls* [Internet]. Treasure Island (FL): StatPearls Publishing; 2019.
26. Ricciotti E, FitzGerald GA. Prostaglandins and inflammation. *Arterioscler Thromb Vasc Biol* 2011; 31:986–1000. [\[Crossref\]](#)
27. Tufan A, Matucci-Cerinic M. COVID-19, immune system response, hyperinflammation and repurposing anti-rheumatic drugs. *Turkish J Med Sci* 2020; 50:620–632. [\[Crossref\]](#)
28. Arlati S. Pathophysiology of acute illness and injury. In: *Operative techniques and recent advances in acute care and emergency surgery*. Springer, 2019; p11–42. [\[Crossref\]](#)
29. Mosevoll KA, Johansen S, Wendelbo Ø, Nepsstad I, Bruserud Ø, Reikvam H. Cytokines, adhesion molecules, and matrix metalloproteases as predisposing, diagnostic, and prognostic factors in venous thrombosis. *Front Med* 2018; 5:147. [\[Crossref\]](#)
30. Khan YS, Lynch DT. Histology, Lung. In: *StatPearls* [Internet]. StatPearls Publishing; 2019.
31. Wilmott RW, Bush A, Deterding RR, et al. *Kendig's disorders of the respiratory tract in children e-book*. Elsevier Health Sciences; 2018.
32. Webb WR, Bronchiectasis. In: Naidich DP, Webb WR, Grenier PA, Harkin TJ, Gefter WB, eds. *Imaging of the airways: functional and radiologic correlations*. 1st ed. Philadelphia: Lippincott Williams & Wilkins, 2005; 106–145.

33. Kim SJ, Im JG, Kim IO, et al. Normal bronchial and pulmonary arterial diameters measured by thin section CT. *J Comput Assist Tomogr* 1995; 19:365–369. [\[Crossref\]](#)
34. Reiff DB, Wells AU, Carr DH, et al. CT findings in bronchiectasis: limited value in distinguishing between idiopathic and specific types. *Am J Roentgenol* 1995; 165:261–267. [\[Crossref\]](#)
35. Jeffery PK. The development of large and small airways. *Am J Respir Crit Care Med* 1998; 157:S174–S180. [\[Crossref\]](#)